2024 IEEE International Conference on Robotics and Automation (ICRA 2024)
May 13-17, 2024. Yokohama, Japan

A Flat Tendon-Driven Continuum Microrobot for Brain Interventions

Lorenzo Noseda[1], Addison Liu[2], Lucio Pancaldi[1] and Mahmut Selman Sakar[1]

***Abstract*— Navigating biomedical instruments inside the brain remains challenging and high-risk. The delicate nature of the tissues involved requires the development of cutting-edge robotic technologies to enhance precision and safety. In response to these demands, this paper presents a novel ribbon-shaped, tendon-driven continuum microrobot designed explicitly to navigate through brain tissues. The microrobot has a cross-sectional area of 1 mm^2, and its design is readily compatible with conventional microfabrication techniques for further miniaturization. The flat geometry aims to provide superior maneuverability and opens up new challenges for modeling and control. We detail the design methodology and fabrication, followed by in vitro characterization and testing within brain tissue phantoms.**

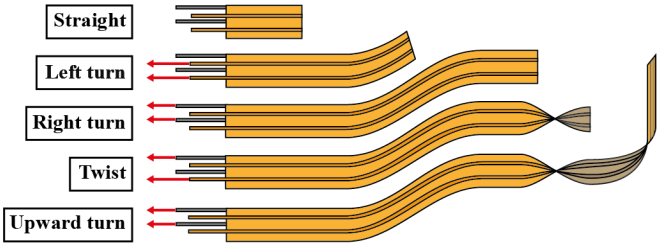

Fig. 1. Envisioned 3D steering mechanism for ribbon-shaped microrobots through coordinated actuation of four tendons. Ribbon-shape unlocks novel deformation modes including twist.

I. INTRODUCTION

Minimally invasive robot-assisted diagnostic and therapeutic tools can have a profound impact on the treatment of neurological diseases and brain tumors, with reduced side effects and increased efficacy [1]–[3]. To this end, miniaturized slender instruments such as needles, cannulas, neural probes, and catheters have widespread uses in research laboratories and clinics.

Continuum robots push minimally invasive navigation to the next level by providing superior maneuverability and safer interactions through mechanical compliance [4]. Robot-assisted steering of flexible needles inside soft tissues has been studied extensively in the context of kinematics, control, and path planning [5]–[10]. When a flexible needle featuring a beveled tip is inserted into soft tissue, the asymmetric design of the tip leads to the needle bending and creating a curved path. By twisting the base, the needle pivots around its axis, which adjusts the orientation of the beveled tip. Alternatively, a number of robots have been developed that involve the use of concentric tubes, tendon-driven mechanisms, and pneumatic chambers [11]. At smaller scales, designs that are comparatively straightforward tend to be more appealing. The use of concentric tubes [12]–[14] and mechanisms driven by tendons [15]–[17] facilitates achieving smaller ratios of diameter to length, where flexible components integrated with transmission lines are employed to eliminate the need for tiny joints and pulleys.

The design and manufacturing scheme of existing continuum robots is not compatible with conventional microfabrication techniques, posing a significant challenge for miniaturization. Fortunately, recent advances in materials science and microengineering realized microscopic probes with integrated electromechanical and fluidic elements that allow long-term monitoring of biological activity at the single-cell level and delivering precise doses of stimulation or therapy to the target tissues [18]–[20]. The primary difference between conventional continuum robots and microengineered probes is the geometry. Instead of having a circular cross-section, microengineered probes can have a rectangular cross-section. The change in the geometry demands novel actuation and steering solutions. The critical buckling force is proportional to the bending stiffness of the structure, while it is inversely proportional to the square of the length. Therefore, ribbon-shaped probes are highly susceptible to bending and buckling [21]. One strategy to facilitate probe insertion is to reinforce the bending stiffness of the device using removable shuttles, dissolvable coatings, and materials with adjustable stiffness [22], [23]. As an alternative strategy, the effective length of the probe can be reduced using rigid braces and surface guides that are positioned at the site of insertion [22], [23]. However, these techniques are only effective if the objective is to insert and deploy the device along a straight trajectory.

To address this unmet technological need, this work introduces a ribbon-shaped (i.e., rectangular cross-section) tendon-actuated device controlled from the proximal end by a robotic micromanipulation system. Ribbons, characterized by their distinct thickness, width, and length, possess the unique ability to deform into configurations unachievable by other slender structures such as rods. We postulate that this geometry could facilitate agile 3D navigation within the brain. Depending on the tendon activation patterns, the ultra-flexible structure will bend or twist at the distal end, moving in the desired direction within the tissue. Additionally, the ribbon shape is advantageous as it displaces smaller volumes of tissue during advancement compared to devices with a circular cross-section of similar width. Finally, employing

[1] are with Institute of Mechanical Engineering, École Polytechnique Fédérale de Lausanne (EPFL), 1015 Lausanne, Switzerland lorenzo.noseda@epfl.ch, lucio.pancaldi@epfl.ch, selman.sakar@epfl.ch
[2] is with John A. Paulson School of Engineering and Applied Sciences, Harvard University, Cambridge, MA, USA ayliu@college.harvard.edu

ribbons enables a design and manufacturing paradigm rooted in flexible electronics and microfluidics technology, paving the way for the development of soft robotic devices that are exceptionally thin yet highly functional.

The system is designed to allow the operator to move the microrobot around anatomical features (e.g., blood vessels, nerve cords) to reach a target region using visual feedback and/or measurements provided by onboard sensors. The base material, polyimide (PI), has been extensively used for the microfabrication of flexible sensors. The whole operation can be automated in the future with the use of proper path-planning algorithms. The envisioned 3D navigation strategy is illustrated in Figure 1. The robot has two main parts: the backbone and the tendons. The device presented in this work has two tendons, one attached at each side of the backbone at its tip. This configuration allows steering in 2D only, yet the simplicity of the design enables rapid and detailed analysis of the problem for the design of future prototypes.

II. METHODS

A. Design and manufacturing of the microrobot

Optimizing the design and accounting for the mechanics of the different parts is necessary for the successful implementation of the main idea. There are several important considerations in order to choose the correct profile for the backbone. If the overall structure is too rigid, the robot will be unable to steer; instead of following the direction of steering, the robot will move in the direction of the push. On the other hand, a floppy structure will result in buckling of the main body during advancement instead of transmission of the proximal push to the distal end. The tendons must transmit tensile forces applied by the motors at the insertion side to the distal end and endure tension in the process. Finally, it is critical to avoid dissection of the tissue, which occurs when tendons detach from the backbone while being pulled.

The prototype shown in Figure 2 is composed of layers of PI film (Kapton HN, Dupont) of variable thickness, which are hand-cut with a razor blade, manually aligned, and glued together. The central layer is 75 μm in thickness and serves as the backbone for the device, providing structural support during insertion into the tissue. The tendons are 50 μm in thickness and are attached at the tip of the device with instant cyanoacrylate glue (Loctite 414). To keep the tendons close to the backbone during steering, a thin 12.5 μm encapsulation layer is added on both sides of the device within the region that is inserted in the brain phantom. It is glued to the backbone edges with a flexible silane-modified polymer-based glue (Loctite Repair Xtreme) to sustain the compliance of the device. The guided region of the device has increased width and thickness to enable feeding without compression of the tendons by the device feeder. The current fabrication method leads to a thickness of approximately 200 μm.

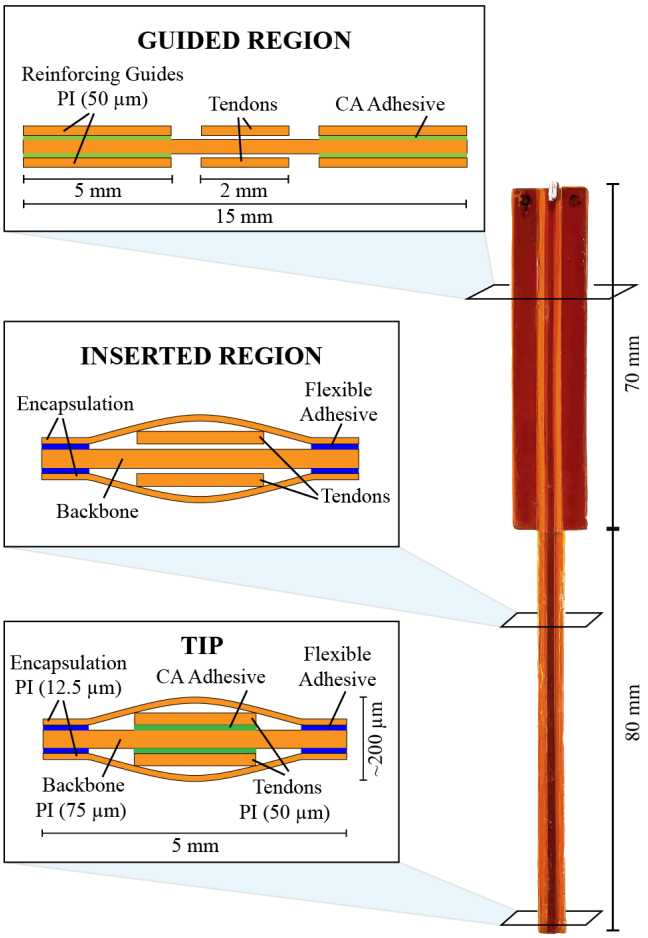

Fig. 2. Photograph of a device (right) with a cross-sectional profile schematically illustrated on the left. The device has three distinct regions that correspond to the distal tip, the functional part that is inserted into, and navigated inside the gel, and the proximal part that is not inserted into the gel but conveyed by the barrels of the robotic micromanipulation system.

B. Robotic micromanipulation system

The primary function of the robotic micromanipulation system is to actuate the tendons in a coordinated fashion while pushing the body forward so that the microrobot can move along the desired trajectory with the desired kinematics. The system must be equipped with a proper imaging suite to provide visual feedback to the human operator. In this work, the microrobot was teleoperated using bright-field images acquired by a CCD camera (Basler acA4024-29uc), observing the workspace from a single plane. The working distance between the lens (Fujinon HF12.5SA-1) and the target is approximately 100 mm.

Figure 3 shows the experimental platform along with an illustration of the advancement scheme. The system provides three controlled axes, two for the tendons and one for the feeder. We aim to keep the system as compact as possible to allow the insertion of the microrobots at any desired location of the tissue. The system consists of three stepper motors (Nema 17) for velocity control with microstepping (16 divisions) for increased resolution and

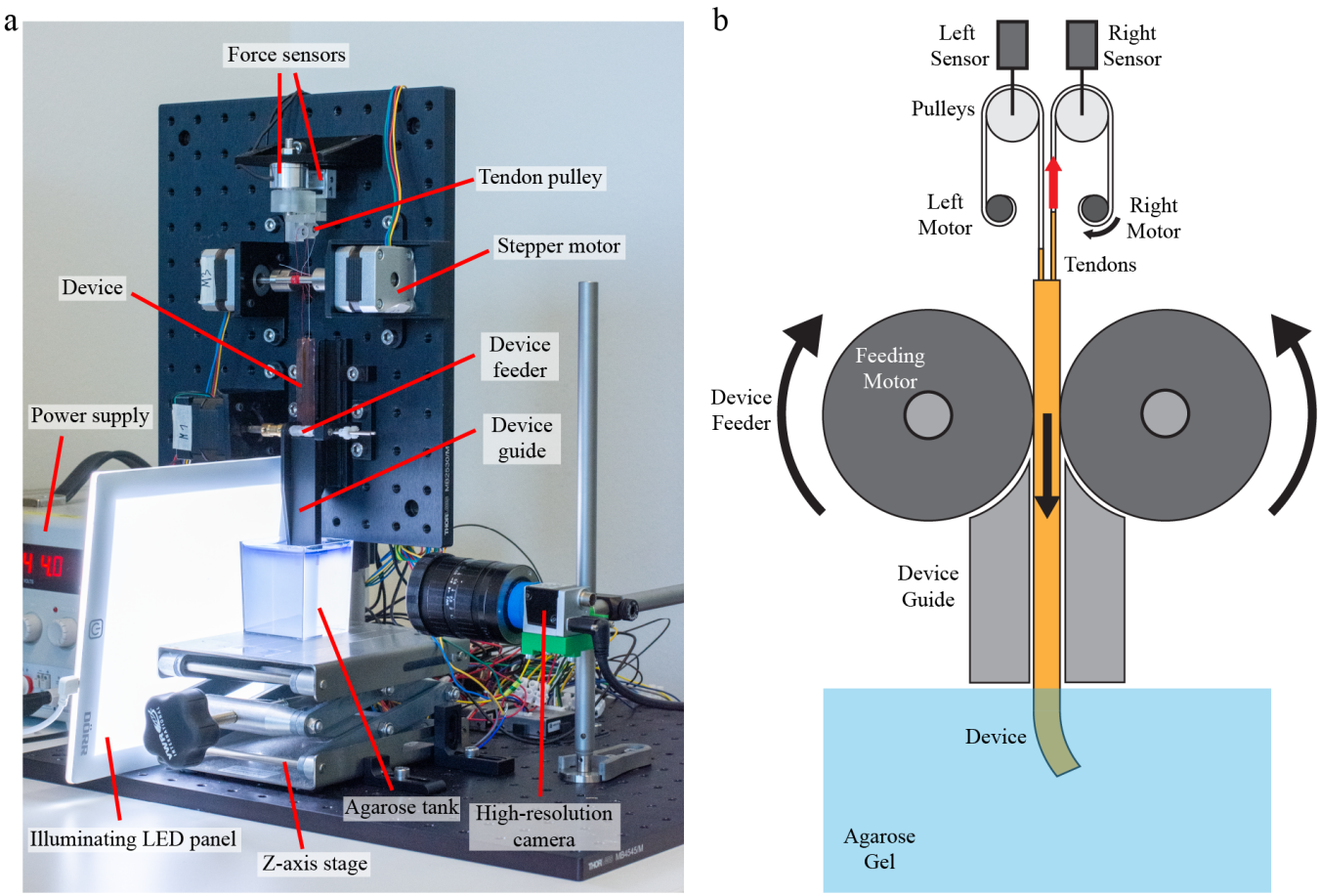

Fig. 3. Robotic micromanipulation system. Several mechanisms are nested into a single system that ensures proper coordination of robot release with steering operation. Accurate and rapid tuning of tension over the tendons is essential for avoiding maneuvers that would result in tissue damage or deviations from the planned trajectory. a. Experimental platform. b. Schematic illustration of the insertion and steering mechanism showing advancement of the device and bending counterclockwise by increasing tension on the right tendon.

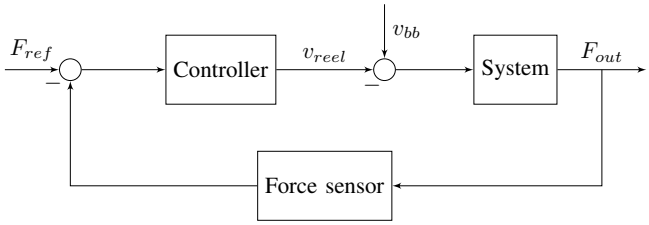

Fig. 4. Closed-loop control of the tension on the tendons. F_{ref} is the reference tension to be applied to the tendons, v_{reel} is the velocity offset calculated by the PID controller, v_{bb} is the insertion velocity of the backbone, F_{out} is the tension applied on the tendons.

two force sensors (KM26z, ME-Meßsysteme) for tendon tension measurements. The feeder consists of two counter-rotating barrels, essentially serving as a conveyor belt. A single motor actuates the barrels through a gear transmission system. Considering the ribbon shape of the device, this mechanism is particularly suited to ensure precise linear motion and avoid mechanical instabilities. The tendons are routed around pulleys, which are connected to force sensors that continuously measure the tension force on the tendons.

In the control architecture of our system, the backbone's advancement velocity is governed by an open-loop control system, which accepts the desired insertion velocity as its input. To be able to control the insertion depth, the advancement is timed. In contrast, the tendons are managed through a closed-loop control system (Fig. 4) designed to maintain a specified tension. This system employs a proportional-integral-derivative (PID) controller that outputs a velocity offset based on the discrepancy between the actual and desired tension levels. This offset is then subtracted from the backbone's advancement velocity to adjust the input velocity to the motors controlling the tendons, thereby regulating the tension within the tendons effectively.

III. RESULTS

A. Characterization of robot navigation

We performed navigation experiments in a 0.6% agarose gel, a phantom that is typically used to mimic the mechanical properties of the brain. The gel is covered with deionized (DI) water to avoid drying. Two drops of ink are added to this layer of DI water to enhance the visualization of the paths followed by the robots.

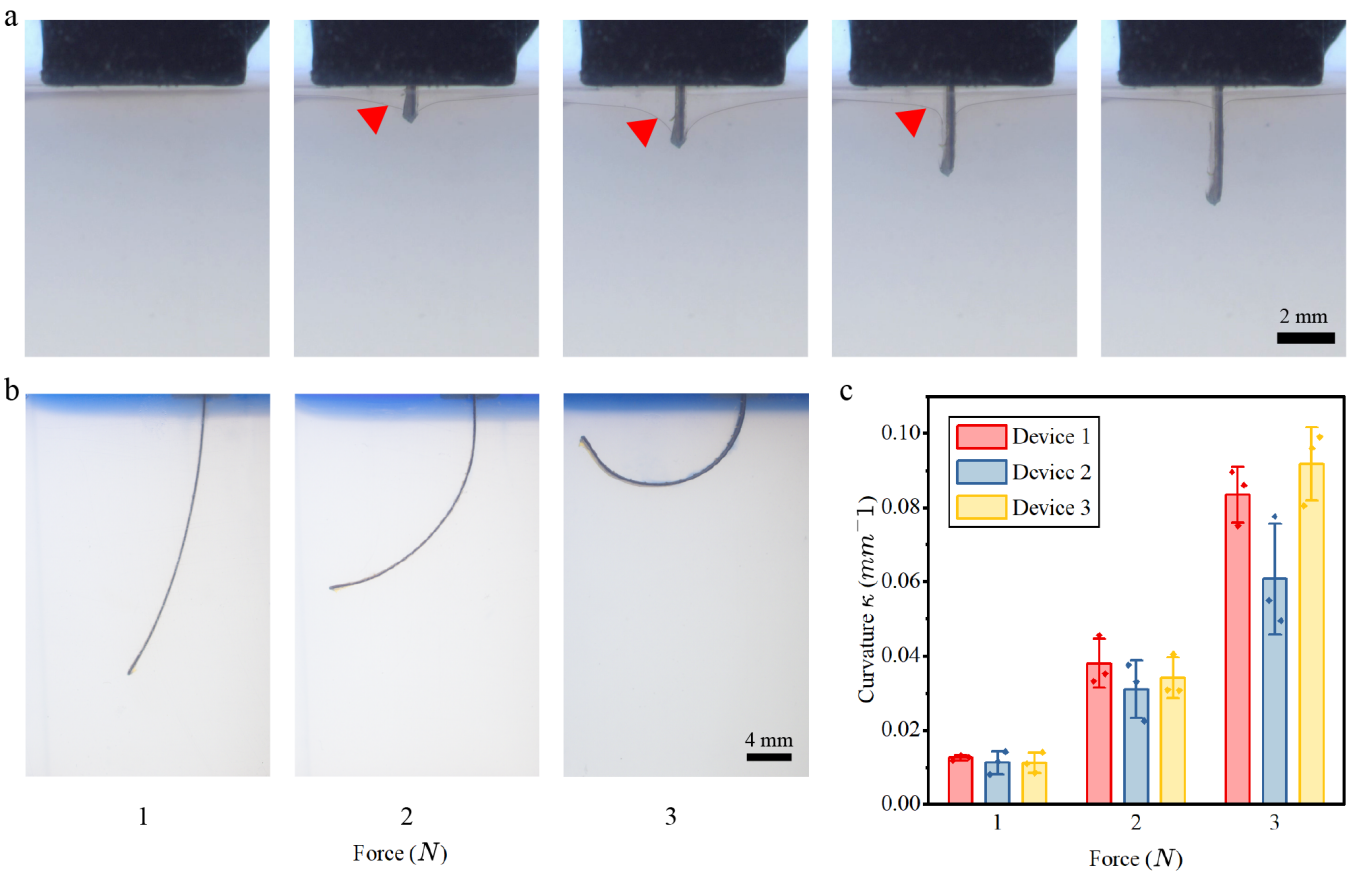

Fig. 5. Insertion and advancement inside a brain phantom. a. Images show different stages of insertion and advancement. First, the guide is positioned on top of the gel. When the robot is pushed against the gel, the interface (red arrow) deforms. Once the maximal indentation is reached, a crack is initiated in the gel. This crack propagates as the robot is pushed further into the gel. b. Representative images of a robot bending clockwise. The right tendon was pulled with 0.2 N while the tension on the left tendon was modulated from 1 N to 3 N. The same forces are applied to the tendons by the PID controller during the advancement. c. Curvature κ as a function of force applied to the tendon. Each trial was repeated 3 times in different phantoms. Bar height indicates the mean value, whiskers show the standard deviation, and dots are the individual data points.

There are two major stages of navigation: insertion of the robot into the phantom and advancement inside the gel. The robot was first inserted for 5 mm into the gel to initiate a crack. To do so, 0.2 N pre-tension was applied on both tendons, which enabled penetration and protected the backbone from buckling. The insertion guide was placed at the gel-water interface (Fig. 5a) and the robot was fed at a speed of 1 $mm \cdot s^{-1}$. When the robot comes in contact with the gel, the indentation phase begins, which involves local compression of the gel. In our experiments, a crack formed after pushing the robot for 2-3 mm, which then led to progressive crack propagation. At this stage, the robot was often slightly tilted with respect to the vertical axis. We believe that the compressive stresses prior to insertion cause a slight bending of the tip, leading to an inclined crack propagation. An improved insertion strategy or tip geometry could address this issue.

After the first 5 mm of straight-line insertion, a pre-defined tension was applied to one of the tendons, while keeping the 0.2 N pre-tension on the other. The device was advanced for another 30 mm at 1 $mm \cdot s^{-1}$. The tests were conducted on three different robots, for which three repetitions were conducted for each robot (1, 2, and 3 N). The average curvature of the robots was extracted from a still image of the workspace using the Fiji plugin Kappa. Representative images of robot bending at the three force levels are shown in Figure 5b and the results for several robots are presented in Figure 5c. The average curvature obtained at 1, 2, and 3 N over three different devices is 0.0116, 0.0344, and 0.0786 mm^{-1}, respectively.

The results show a strong correlation between the curvature and the applied force, validating the steering capability of the robot. Nevertheless, there are some non-negligible variations, both intra and inter-device, at each force level. We believe the latter to be a consequence of the current fabrication method, where PI layers were manually aligned and glued under a stereomicroscope. Regarding the intra-device variation, the cracking behavior of agarose could be a cause, as well as shortcomings in the sensing and application of forces. Ideally, we would want to sense and control the force applied by the device on the tissue at the tip. However, since the sensor is connected to the tendon externally, the force reading is impacted by friction on the tendon throughout its routing, which could, in turn, be

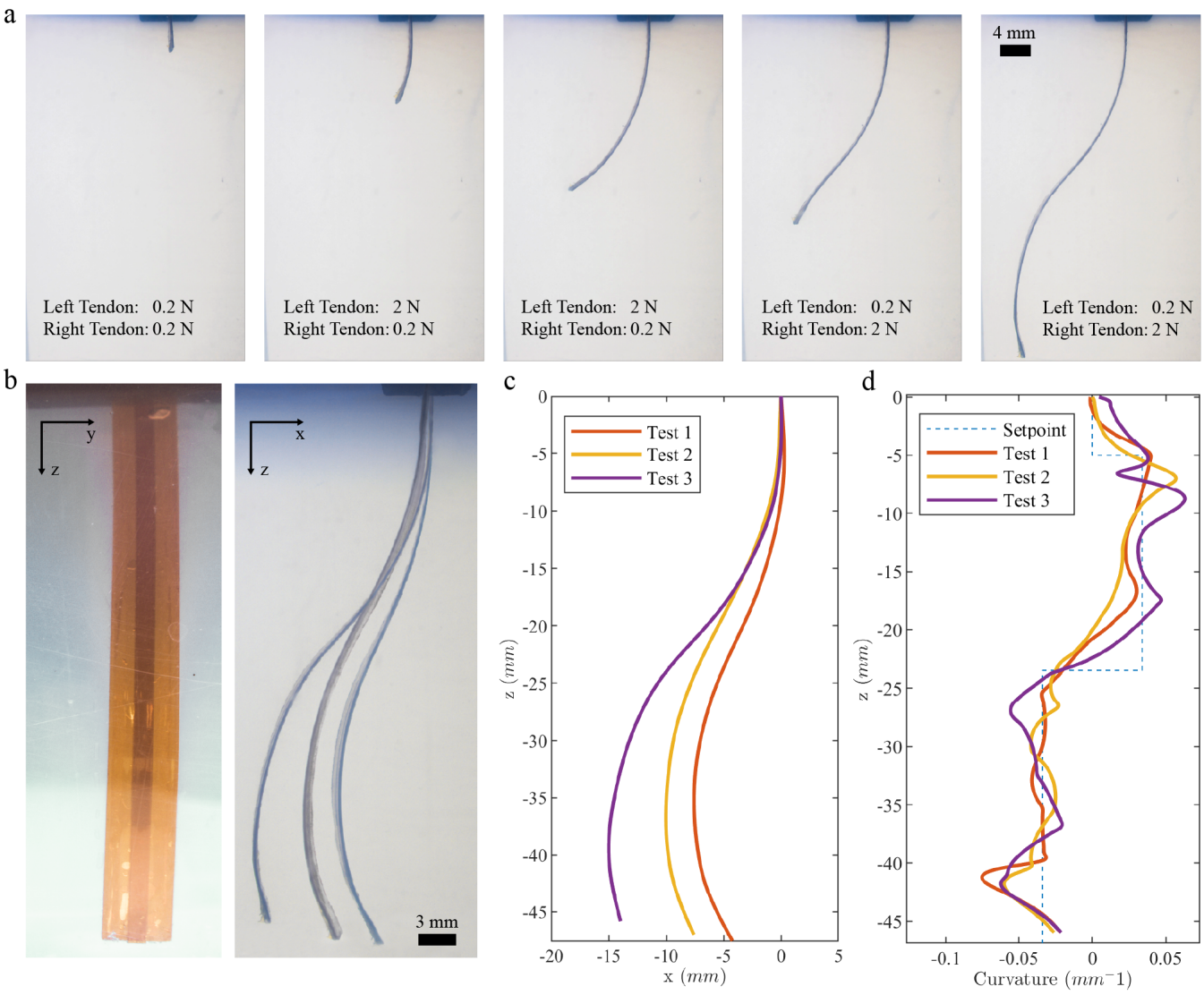

Fig. 6. Open-loop automated navigation. a. Time-lapse images showing the advancement of the robot along a curved path. The curvature is updated twice by the controller after moving the robot straight. b. An image showing a single robot from the side view (left) and the superposition of the images from three different trials, each conducted at different locations in the gel. c. The digitized version of the robot poses at the end of the three navigation trials. d. The curvature of the robot at the end of the navigation trial along the axis of penetration. Noise in the data was removed using a 3rd order low-pass Butterworth filter. The dashed line (Setpoint) represents the curvature input to the controller.

impacted by the curvature of the robot. A potential solution to overcome this will be the introduction of a closed-loop control strategy based on visual feedback on the position or the curvature.

B. Open-loop automated navigation

We conducted an experiment consisting of two consecutive turns in opposite directions to test the ability of the robot to navigate in an open-loop fashion. As shown in Figure 6a, the robot was first inserted straight for 5 mm, then curved clockwise along a 20 mm path, and finally curved counterclockwise for the last 25 mm, both with a pre-defined curvature of 0.034 mm^{-1}. This pre-set curvature corresponds to the application of 2 N to one of the tendons while keeping a pre-tension of 0.2 N on the other.

A side-view of one of the trials, along with the superposition of images from three different trials that were performed with the same device at three different locations in the agarose gel is shown in Figure 6b. The curves were digitized using the Fiji Kappa plugin and imported to MATLAB (Fig. 6c). Visual inspection of the different paths shows a misalignment in the initial straight-line motion. As explained previously, crack initiation can impact the initial alignment of the robot. To better understand the sources of the error, we graphed the curvature as a function of the path length against the reference curvature (Fig. 6d). Although the curvature in the three tests is close to the reference curvature, there are fluctuations along the trajectory. These fluctuations could be generated by inhomogeneities in the gel, crack propagation, and disturbances in the application of tension

on the tendons. The data further indicates that a sharp change in the curvature of the distal part of the device significantly affects the curvature of the proximal part. Specifically, the average curvatures measured for the first and second turns were 0.024 mm^{-1} and of 0.038 mm^{-1}, respectively. The alteration in pose will be considered in the development of future controllers.

IV. DISCUSSION

We introduced a ribbon-shaped, tendon-driven microrobot to provide a solution for minimally invasive neurosurgical interventions and introduce a novel class of multi-functional microengineered devices with on-board electronics. The use of thin PI films as the core structural element not only grants superior flexibility but also opens the door for integrating electronics through standard microfabrication techniques that involve deposition and etching of materials. With on-board electronics, real-time localization and autonomous steering towards pathological regions will become feasible without relying on visual servoing, thereby pushing the boundaries of what is currently achievable in brain interventions.

In-vitro tests in a brain phantom have demonstrated the navigation capabilities of the device, opening the road to 3D teleoperation and eventually to fully automated operation. The first crucial step was the successful insertion of the device into the soft tissue. The observed initial deviations during insertion provide valuable insights that will guide future efforts to refine and optimize the device's performance. As we delve deeper into understanding and addressing these deviations, we anticipate even greater precision and reliability in our navigation capabilities. Moving forward, our work will include a more in-depth characterization of the steering capabilities, with particular attention to 3D navigation.

Furthermore, we demonstrated the device's ability to generate paths with varying curvatures. This flexibility in path generation is vital for maneuvering through the complex neural networks of the brain. While there is some variability in these paths, acknowledging this allows us to focus on future improvements through design and the introduction of feedback control. These measures will undoubtedly contribute to increased accuracy and reduced tissue damage during navigation. We postulate that a ribbon-shaped microscopic device may be transported and retracted within tissues with minimal operative damage. The tissues may spontaneously heal such small dissections, minimizing the scar tissue left behind by the device. Our future work will include experiments with living tissues to assess the ease of navigation and extent of tissue damage. We will perform finite element simulations to refine our device design, enhance its functionality, and ensure a more gentle interaction with biological tissues.

REFERENCES

[1] J. J. Doulgeris, S. A. Gonzalez-Blohm, A. K. Filis, T. M. Shea, K. Aghayev, and F. D. Vrionis, "Robotics in neurosurgery: evolution, current challenges, and compromises," *Cancer Control*, vol. 22, no. 3, pp. 352–359, 2015.

[2] C. Beaman, N. Kaneko, P. Meyers, and S. Tateshima, "A review of robotic interventional neuroradiology," *American Journal of Neuroradiology*, vol. 42, no. 5, pp. 808–814, 2021.

[3] B. J. Nelson, S. Gervasoni, P. W. Chiu, L. Zhang, and A. Zemmar, "Magnetically actuated medical robots: An in vivo perspective," *Proceedings of the IEEE*, vol. 110, no. 7, pp. 1028–1037, 2022.

[4] T. da Veiga, J. H. Chandler, P. Lloyd, G. Pittiglio, N. J. Wilkinson, A. K. Hoshiar, R. A. Harris, and P. Valdastri, "Challenges of continuum robots in clinical context: a review," *Progress in Biomedical Engineering*, vol. 2, no. 3, p. 032003, 2020.

[5] S. P. DiMaio and S. E. Salcudean, "Needle steering and motion planning in soft tissues," *IEEE Transactions on Biomedical Engineering*, vol. 52, no. 6, pp. 965–974, 2005.

[6] R. J. Webster III, J. S. Kim, N. J. Cowan, G. S. Chirikjian, and A. M. Okamura, "Nonholonomic modeling of needle steering," *The International Journal of Robotics Research*, vol. 25, no. 5-6, pp. 509–525, 2006.

[7] D. Glozman and M. Shoham, "Image-guided robotic flexible needle steering," *IEEE Transactions on Robotics*, vol. 23, no. 3, pp. 459–467, 2007.

[8] M. Mahvash and P. E. Dupont, "Mechanics of dynamic needle insertion into a biological material," *IEEE Transactions on Biomedical Engineering*, vol. 57, no. 4, pp. 934–943, 2009.

[9] K. B. Reed, A. Majewicz, V. Kallem, R. Alterovitz, K. Goldberg, N. J. Cowan, and A. M. Okamura, "Robot-assisted needle steering," *IEEE robotics & automation magazine*, vol. 18, no. 4, pp. 35–46, 2011.

[10] T. Watts, R. Secoli, and F. R. y Baena, "A mechanics-based model for 3-d steering of programmable bevel-tip needles," *IEEE Transactions on Robotics*, vol. 35, no. 2, pp. 371–386, 2018.

[11] J. Burgner-Kahrs, D. C. Rucker, and H. Choset, "Continuum robots for medical applications: A survey," *IEEE Transactions on Robotics*, vol. 31, no. 6, pp. 1261–1280, 2015.

[12] R. J. Webster, J. M. Romano, and N. J. Cowan, "Mechanics of precurved-tube continuum robots," *IEEE transactions on robotics*, vol. 25, no. 1, pp. 67–78, 2008.

[13] P. E. Dupont, J. Lock, B. Itkowitz, and E. Butler, "Design and control of concentric-tube robots," *IEEE Transactions on Robotics*, vol. 26, no. 2, pp. 209–225, 2009.

[14] D. C. Rucker, R. J. Webster III, G. S. Chirikjian, and N. J. Cowan, "Equilibrium conformations of concentric-tube continuum robots," *The International journal of robotics research*, vol. 29, no. 10, pp. 1263–1280, 2010.

[15] D. B. Camarillo, C. R. Carlson, and J. K. Salisbury, "Configuration tracking for continuum manipulators with coupled tendon drive," *IEEE transactions on robotics*, vol. 25, no. 4, pp. 798–808, 2009.

[16] S. Y. Ko, L. Frasson, and F. R. y Baena, "Closed-loop planar motion control of a steerable probe with a "programmable bevel" inspired by nature," *IEEE Transactions on Robotics*, vol. 27, no. 5, pp. 970–983, 2011.

[17] E. Amanov, T.-D. Nguyen, and J. Burgner-Kahrs, "Tendon-driven continuum robots with extensible sections—a model-based evaluation of path-following motions," *The International Journal of Robotics Research*, vol. 40, no. 1, pp. 7–23, 2021.

[18] R. Chen, A. Canales, and P. Anikeeva, "Neural recording and modulation technologies," *Nature Reviews Materials*, vol. 2, no. 2, pp. 1–16, 2017.

[19] J. A. Frank, M.-J. Antonini, and P. Anikeeva, "Next-generation interfaces for studying neural function," *Nature biotechnology*, vol. 37, no. 9, pp. 1013–1023, 2019.

[20] A. Vázquez-Guardado, Y. Yang, A. J. Bandodkar, and J. A. Rogers, "Recent advances in neurotechnologies with broad potential for neuroscience research," *Nature neuroscience*, vol. 23, no. 12, pp. 1522–1536, 2020.

[21] K. B. Ramadi and M. J. Cima, "Materials and devices for microinvasive neural interfacing," *MRS Advances*, vol. 4, no. 51-52, pp. 2805–2816, 2019.

[22] B. Thielen and E. Meng, "A comparison of insertion methods for surgical placement of penetrating neural interfaces," *Journal of neural engineering*, vol. 18, no. 4, p. 041003, 2021.

[23] S. Zhang, C. Wang, C. Linghu, S. Wang, and J. Song, "Mechanics strategies for implantation of flexible neural probes," *Journal of Applied Mechanics*, vol. 88, no. 1, p. 010801, 2021.